Journal of Electronic Materials (2022) 51:2256–2265
https://doi.org/10.1007/s11664-022-09477-y

ORIGINAL RESEARCH ARTICLE

Improvement of Contact and Bonding Performance of Mg_2Si/Mg_2SiNi_3 Thermoelectric Joints by Optimizing the Concentration Gradient of Mg

Shaoping Chen[1] · Jie Chen[1] · Wenhao Fan[2] · Yaning Wang[1] · Jingyun Guo[1] · Yachao Wang[1] · Yu Jiang[2] · Rasha Abdullah Ahmed Al-Yusufi[2] · Marhoun Ferhat[3]

Received: 6 November 2021 / Accepted: 24 January 2022 / Published online: 21 February 2022
© The Minerals, Metals & Materials Society 2022

Abstract

Mg_2SiNi_3, is a topologically densely packed intermetallic compound (TCP-IMC) and an excellent diffusion barrier material between nickel and Mg_2Si-based thermoelectric material. However, even a little migration of the Mg atom from Mg_2Si to Mg_2SiNi_3 under the action of a driven force promotes the formation of an Mg deficiency region on the Mg_2Si side, which destroys the balance of point defects and leads to performance deterioration. In this work, by adjusting the chemical potential of Mg across the $Mg_xSi_{15}Ni_{50}/Mg_2Si$ (x = 36, 50, 130) interface, the migration of Mg in thermoelectric material has been suppressed effectively. The results indicate that the contact performance and service stability of the $Mg_{130}Si_{15}Ni_{50}/Mg_2Si$ interface has been improved by 50% compared to that of $Mg_{36}Si_{15}Ni_{50}/Mg_2Si$, which remains quite well after annealing at 400 ℃ for 480 h. TCP-IMC barrier with proper composition is a promising design for the manufacture of TEG interface to ensure its consistency in service especially under a large temperature difference.

Keywords Thermoelectric joints · Mg_2Si · Mg_2SiNi_3 · concentration gradient · contact resistivity · shear strength

Introduction

As a new kind of clean energy conversion technique, thermoelectric power generators (TEG) can directly convert waste heat into electric energy and improve the efficiency of energy usage based on Seebeck effect. They have been applied in a wide range of fields including the recovery and utilization of industrial waste heat and deep-space exploration.[1,2] A large number of materials with $zT > 1$ have been reported, e.g., nanostructured PbTe, $CoSb_3$ -based skutterudites, half-Heuslers, SnSe, Cu_2Se-based materials, and Mg_2Si-based solid solutions, which have potential prospect for use in the mid-temperature region between 500 K and 800 K.[3]

In recent years, the performance of thermoelectric materials has continued to make breakthroughs, which is determined by the dimensionless figure of merit,[4] $zT = S^2\sigma T/k$,[5–7] where σ is the electrical conductivity, S is the Seebeck coefficient, k is the thermal conductivity and T is the absolute temperature. When the temperature difference reaches 350 K, the theoretical value of thermoelectric conversion efficiency of thermoelectric materials with average zT between 1 and 2 is about 10%.[8] However, these high values never translate adequately into the performance of devices, mainly due to challenges in making stable contact between thermoelectric material and electrodes. To realize a stable contact between thermoelectric material and electrodes, a barrier layer is usually applied. However, due to the inevitable mutual diffusion reaction at the interface of the barrier and thermoelectric material, there is still a long way to improve the interface contact by designing proper barrier materials. Furthermore, it must be pointed out that the interfacial reaction, usually accompanied by atomic diffusion across the interface, could be more critical for the magnesium-based TEG working in the mid-temperature region. It has been proved that a deficiency of Mg may deteriorate the performance of the thermoelectric materials[4,9] and contact to the electrode[10,11] as well. So, it is necessary to inhibit the diffusion of elements

✉ Shaoping Chen
chenshaoping@tyut.edu.cn

1 College of Materials Science and Engineering, Taiyuan University of Technology, Taiyuan 030024, China

2 College of Physics and Optoelectronics, Taiyuan University of Technology, Taiyuan 030024, China

3 The University of the West Indies, Kingston 7, Mona, Jamaica

between thermoelectric material and electrodes by adjusting the chemical composition gradient across the interface.

For thermoelectric devices, in addition to the performance of the thermoelectric material itself, contact resistance and bonding strength of the interface between thermoelectric materials and electrodes also have great influence on the efficiency, stability and life of thermoelectric devices.[12,13] In the cases of waste heat harvesting from the vehicle transport and furnace operation, the thermal interfacial resistance of the interface of the diffusion barrier materials and thermoelectric materials are not critical.[14] So, as shown in Eq. 1,[10] contact resistance is one of the main key factors that reduces the effective $\langle ZT\rangle_D$ of thermoelectric devices.

$$\langle ZT\rangle_D = \left(L/\left(L + 2R_c\sigma\right)\right)\langle zT\rangle_M \tag{1}$$

where L and σ are the length and electrical conductivity of the thermoelectric leg, respectively, R_c is the contact resistivity, and $\langle zT\rangle_M$ is the average zT of the thermoelectric material between T_h and T_c. Usually, the ratio of contact resistance to total leg resistance of less than 10% is acceptable. For a typical device, R_c should be much less than $L/2\sigma$ or 10^2 μΩ·cm^2.[10]

Mg_2Si-based thermoelectric material, as a very promising thermoelectric material with a zT up to 1.45,[15–17] has been attracting more attention of scientists committing to its popularization and application as a medium-temperature TEG. As a defective compound, its transport behavior is determined by the concentration of intrinsic point defects, which is closely related to the stoichiometric ratio of elements.[18,19] The mutual diffusion and reaction occurring across the interface destroys the balance of point defects and causes the increase of interface resistance and deterioration of efficiency and even failure due to mechanical damage.[10] In our recent work, it has been shown that Mg_2SiNi_3 is an excellent diffusion barrier between Cu electrodes and Mg_2Si, which not only effectively blocks the diffusion of Cu from the electrode to Mg_2Si thermoelectric material, but also ensures the maximum shear strength (28.29 MPa).[20] It is especially worth mentioning that the contact resistance between the intrinsic Mg_2Si and Mg_2SiNi_3 is pretty low compared to that reported in the literature.[20] However, the influence of the chemical potential of Mg in the interface of Mg_2SiNi_3/Mg_2Si on the dynamic equilibrium of point defects and thermoelectric transport must be further discussed and clarified.

Figure 1 illustrates the complex crystal structure of the Mg_2SiNi_3 material. Mg_2SiNi_3 is a reaction product between Mg_2Si and Ni, with $R\bar{3}m$ space group structure, which belongs to the μ phase in the topologically densely packed intermetallic compound (TCP-IMC).[21] In the space unit, the coordination numbers of Mg, Si, and Ni are 15,12,12, respectively, and the packing ratio is as high as 0.85. It is very dense and stable in air even at 300 °C.[22] The introduction of Mg_2SiNi_3 to form TE/TCP-IMC interface is thought to improve the contact and stability of the interface by suppressing the chemical potential of diffusion and reaction in both thermodynamics and dynamics. Additionally, the dual-bond characteristics of metallic bond and covalent bond is helpful to decrease interface residual stress due to mismatch as well. In this work, Mg_2SiNi_3 is used as a barrier to prepare $Mg_2Si/Mg_xSi_{15}Ni_{50}$ (x=36,50,150) thermoelectric joints to discover how the composition gradient affects the interface diffusion between Mg_2Si and Mg_2SiNi_3. The contact resistance, strength and thermal stability of these joints were studied in detail.

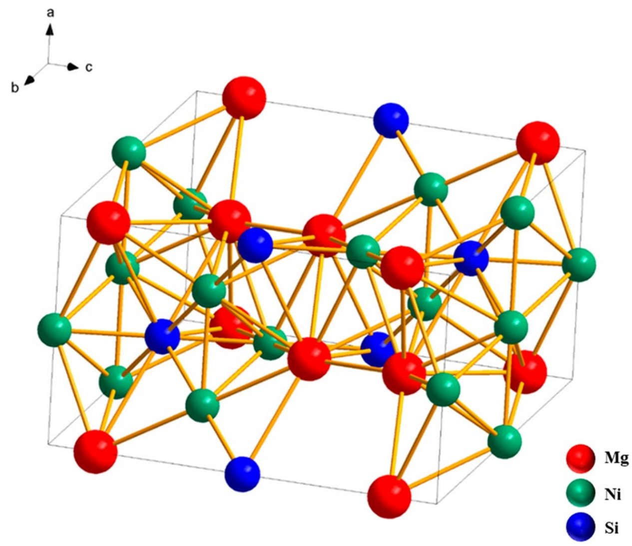

Fig. 1 The crystal structure of the Mg_2SiNi_3 material.

Experimental Procedure

Magnesium powder (≤50 μm, 99.5% pure, Aladdin, Shanghai), silicon powder (≤45 μm, 99.5% pure, Aladdin, Shanghai) and nickel powder (≤45 μm, 99.5% pure, Kermel, Tianjin) were ball mixed for 30 min in stoichiometric ratios of Mg:Si=1.8:1, Mg:Si=2:1 and Mg:Si:Ni=x:15:50 (x=36, 50, 130), respectively, in a high-speed ball mill (QM-3B) with a ball-to-powder mass ratio of 10:1 to obtain $Mg_{1.8}Si$, Mg_2Si and Mg_2SiNi_3.

The milled powders of thermoelectric materials were then cold-pressed inside a graphite die to obtain a green pellet (a diameter of 20 mm). The sample was sintered in a spark plasma sintering apparatus (SPS-630Lx) under sintering temperature 750 °C, uniaxial pressure of 40 MPa and vacuum of 20 Pa. The milled powders of thermoelectric and intermediate materials were then cold-pressed inside a graphite die to obtain a pellet (a diameter of 20 mm) with a symmetrical structure of $Mg_xSi_{15}Ni_{50}/Mg_2Si$ (x=36, 50, 130).

SPS is conducted in vacuum by heating to 630 °C at a speed of 100 °C/min under 10 MPa followed by a 2-min dwell, and then rapidly heating to 750 °C under 40 MPa and staying for another 15 min. During cooling, the temperature was first decreased to 400 °C at a speed of 12.5 °C/min, and then decreased to room temperature at a speed of 10 °C/min. All handling was performed under a protective argon atmosphere.

A thermomechanical analyzer (DIL 402SU, NETZSCH) was used to measure the CTEs of $Mg_xSi_{15}Ni_{50}$(x=36,50,150). The microstructure and chemical composition of thermoelectric joints before and after aging were determined with scanning electron microscopy (SEM, JEOL JSM 6300) and energy dispersive spectroscopy (EDS, HKL). Contact resistance of samples was measured with the four-probe method and the samples for this evaluation were 3×3×δ mm in dimension, with δ being the thickness of the sample, typically 4-5 mm. The phase purity of the thermoelectric materials was confirmed by X-ray diffraction (DX-2700). The Seebeck coefficient and resistivity were performed in a Namicro3 system. A Hall effect test system (CH-100) was used to measure the carrier concentration. The shear strength of samples was tested by a microcomputer-controlled electronic universal testing machine (DNS200) with a head movement rate of 0.5 mm min^{-1}. The samples used for this evaluation were 7×7×δ mm in dimension (δ = 4-5 mm). The joints samples were heat-treated at 400 °C for 120, 240, 360 and 480 h under vacuum of 10^{-4} Pa to evaluate the thermal stability.

Results and Discussion

The Presence and the Influence of Mg-Depletion Layer

As shown in Fig. 2a, the interface of the $Mg_{36}Si_{15}Ni_{50}/Mg_2Si$ thermoelectric joint is a sandwich-like structure. The gray part on the right is the diffusion barrier Mg_2SiNi_3 phase, and the dark layer on the left is the Mg_2Si thermoelectric material. No voids or cracks were observed in the joints. Figure 2b shows a uniform and dense diffusion layer formed in

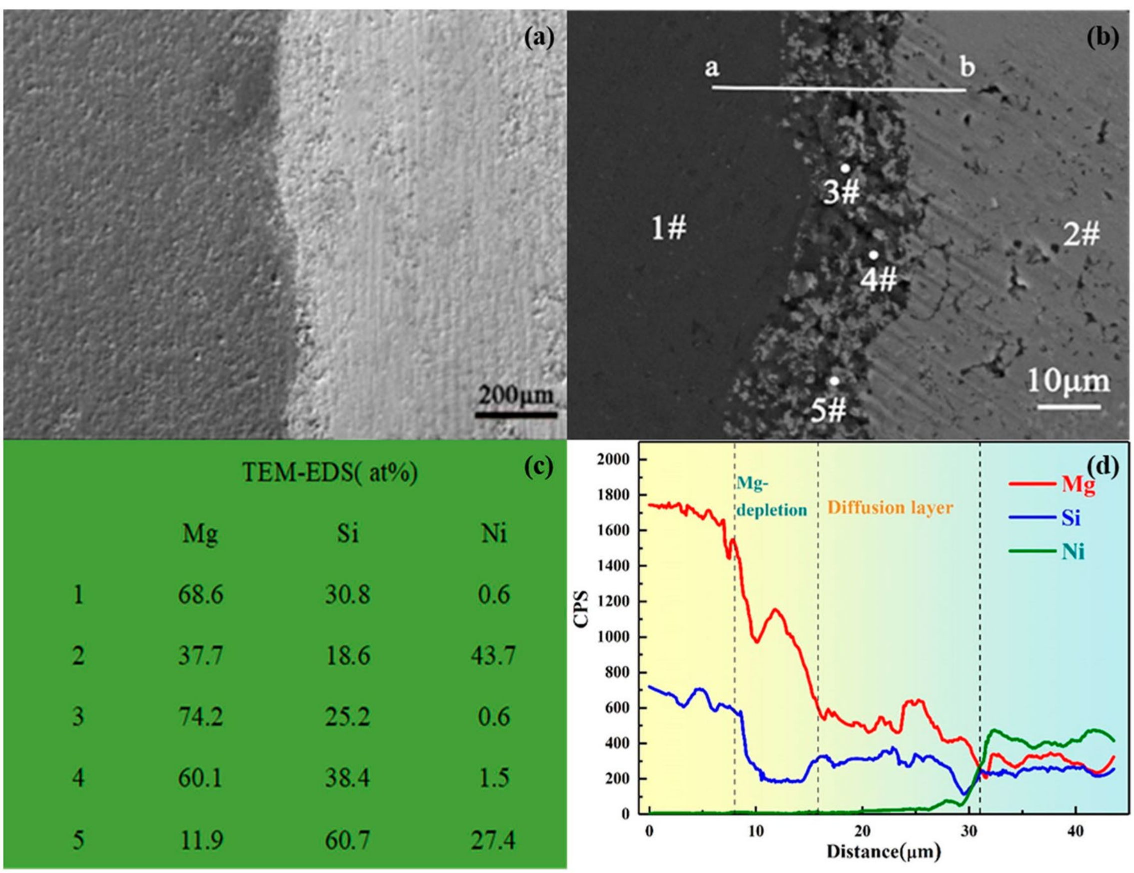

Fig. 2 $Mg_{36}Si_{15}Ni_{50}/Mg_2Si$ thermoelectric joint interface micromorphology (a), (b) micromorphology (c) EDS point analysis results (d) EDS line analysis results of line ab in (b).

the $Mg_2Si/Mg_{36}Si_{15}Ni_{50}$ interface with a thickness of about 15 μm. There are two different phases in the diffusion layer: dark phase and dispersed particles. Combined with EDS analysis (see Fig. 2c) and Mg-Ni-Si ternary phase diagram,[23] it is shown that the atomic ratios of Mg, Si, and Ni at different site are very different, the phase component of matrix of the diffusion layer is basically a mixture of Mg_2Si and Mg, and the second phase particles is $NiSi_2$ phase.[24] EDS analysis result (see Fig. 2d) indicates that a Mg-depletion region (MDR) exists next to the thermoelectric material with a thickness of 7 μm, which is detrimental to the thermoelectric properties of Mg_2Si (discussed below). The formation of MDR is mainly due to faster diffusion velocity of Mg than Si. It is generally accepted that substitutional migration of atoms in intermetallic compounds occurs by virtue of vacancy-type defects. In such an antifluorite-type structure ($Fm\bar{3}m$), sublattice of Si in Mg_2Si can also be viewed as simple cubic with one Si atom of every two missing, so Mg diffuses faster than Si element and is easier to lose.[25] So it would be helpful to suppress the migration of Mg by increasing the percentage of Mg in the barrier and decreasing its ingredient gradient as well. Figure 3a shows the variation of lattice parameters of $Mg_xSi_{15}Ni_{50}$ ($36 \leq x \leq 130$). Linear variation follows the Vegard's law up to x=45, subsequently saturating between x=45 and x=50. Partially squeezed out liquid from the interface may be observed when $x \geq 55$, which is Mg (see Fig. 3b).

Influence of Mg Defect

Because of the high vapor pressure of Mg and high sintering temperature of Mg_2Si, it is difficult to accurately control the stoichiometry of Mg.[26] The excess or lack of magnesium in Mg_2Si affects the balance of the intrinsic defects (I^{Mg},[27] V^{Mg} [28] and anti-defects), thus affecting the electrical properties. In order to study the influence of Mg content on the electrical properties of the material, $Mg_{1.8}Si$ and Mg_2Si were made by SPS. As shown in Fig. 4a, all of diffraction peaks can be indexed to the antifluorite structure (PDF#35-0773; $a = b = c = 6.351$ Å), with a small amount of MgO. The study on the stability and electronic properties of point defects and multivacancies in Mg_2Si shows that the stability of the defects is strongly dependent on the stoichiometric conditions.[29] The V^{MgSi}, V^{Mg2Si} and I^{Mg} are the most stable defects when Mg is rich, while the antisite Si^{Mg} becomes more stable, and I^{Mg} becomes less stable when Mg is poor. Mg_2Si is always n-type in experiments, so the most stable defect is I^{Mg}, which acts as a donor. In stoichiometric conditions, the I^{Mg} defect becomes less favorable, whereas the V^{Mg} defect becomes more stable and the multivacancies are still very favorable.[4] The temperature-dependent electrical properties of $Mg_{1.8}Si$ and Mg_2Si indicate a non-degenerate feature, as shown in Fig. 4b and c. The higher resistivity of the $Mg_{1.8}Si$ sample can be ascribed to the formation of V^{Mg} and loss of the I^{Mg} due to lack of Mg.[30] V^{Mg} has a significant effect on the electric properties of Mg_2Si. In stoichiometric conditions, the formation energy of V^{Mg} is as low as 1.54 eV.[29] This is one of the reasons that the magnesium atoms diffuse very easily. Our recent work shows that the use of intermetallic compounds as a barrier may block the diffusion of Mg effectively.[20]

Suppressing Mg Deletion Through Ingredient Gradient Design

Suppression of the excessive diffusion of Mg atoms in thermoelectric materials can alleviate the generation of Mg vacancies and improve the interface performance. In order to study the effect of the percentage Mg content in the barrier on the net diffusion of interface elements, thermoelectric joints with different concentration gradients ($Mg_xSi_{15}Ni_{50}/Mg_2Si$; x=36,50,130) were designed.

Figure 5a and c presents the microstructures of $Mg_{130}Si_{15}Ni_{50}/Mg_2Si$ and $Mg_{50}Si_{15}Ni_{50}/Mg_2Si$ joints. A

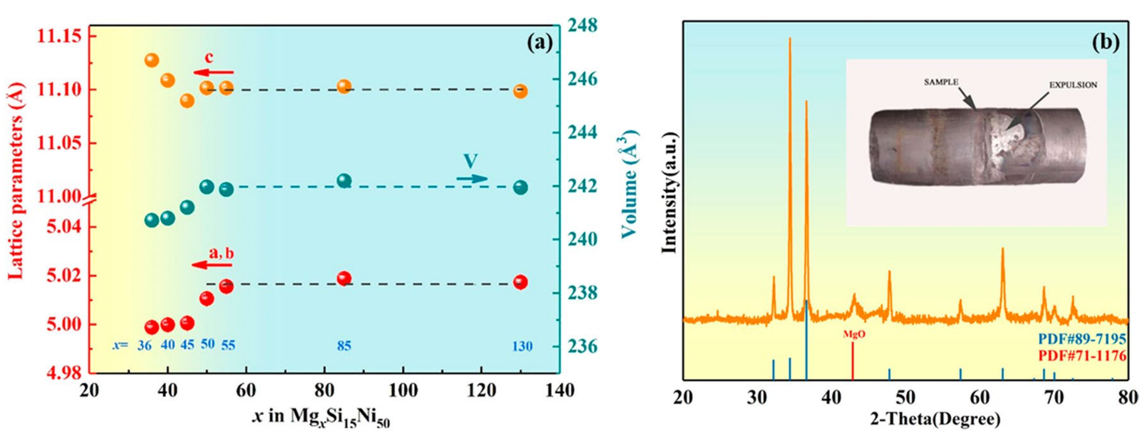

Fig. 3 (a) lattice constant of $Mg_xSi_{15}Ni_{50}$ ($36 \leq x \leq 130$) sample (b) sample with Mg squeezed out during sintering.

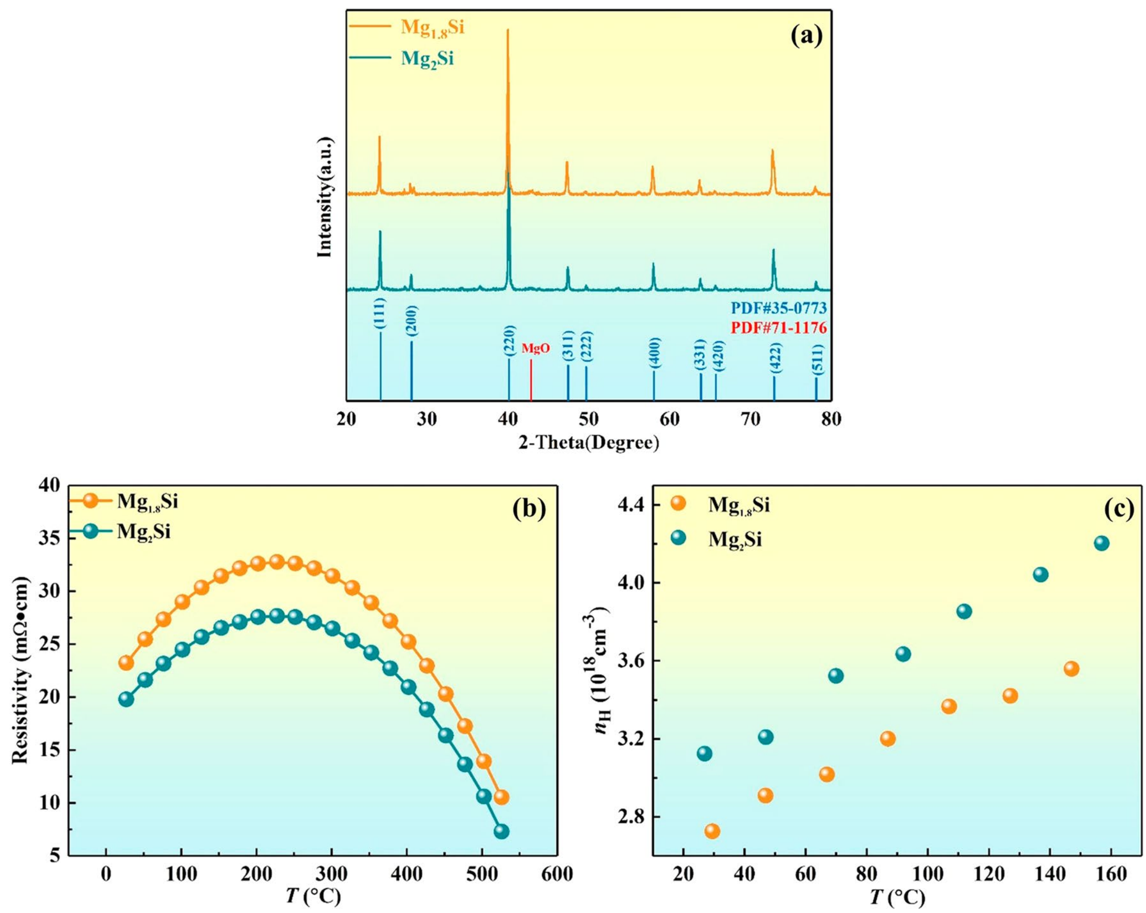

Fig. 4 (a) Room-temperature XRD patterns, (b) Resistivity and (c) Carrier concentration of $Mg_{1.8}Si$ and Mg_2Si.

dense and uniform intermediate layer is formed between the thermoelectric material and the barrier layer with a thickness of 10 μm and 15 μm, respectively. The chemical composition of the diffusion layer is Mg:Si:Ni≈1:1:1, which is close to ω-$(Mg_{0.52}Ni_{0.48})_7Si_4$ phase according to the phase diagram and literature.[28] The EDS results show a diffusion layer next to thermoelectric material as thin as 2 to 3 μm, and no MDR is observed, as shown in Fig. 5b and d, which proves that increasing Mg concentration gradient across the interface by increase of Mg content in Mg_2SiNi_3 side can effectively suppress the Mg loss in the Mg_2Si effectively. Furthermore, when x increases from 50 to 130, no obvious effect is observed in either interface but excess squeezed-out liquid Mg is present in the former sample.

According to Fick's first law of diffusion, the flux of Mg atom from Mg_2Si to $Mg_{36}Si_{15}Ni_{50}$ is given by:

$$J = (-D_0 \Delta C)/\Delta x \quad (2)$$

where D_0 is the diffusion coefficient of Mg in the reaction layer, Δc is concentration difference of c_{Mg_2Si}-$c_{Mg_{36}Si_{15}Ni_{50}}$, Δx is the thickness of reaction layer (15 μm). The per second total number of Mg atom diffusion from Mg_2Si to $Mg_{36}Si_{15}Ni_{50}$ is calculated by

$$J_{total} = J \cdot S \quad (3)$$

where S is the cross-section of the interface. The per second amount of Mg atoms diffused from the $Mg_{36}Si_{15}Ni_{50}/Mg_2Si$ interface is calculated by

$$J_{sec} = J_{total}/C_{(Mg_2Si)} \quad (4)$$

where c_{Mg_2Si} is concentration of Mg in Mg_2Si (3.1×10^{22} at./cm^3). In Mg_2Si, the thickness increase per second of the Mg-poor layer is calculated by

$$\Delta l_{Sec} = J_{sec}/S \quad (5)$$

Therefore, the thickness of the Mg-poor layer in Mg_2Si is calculated by

$$\Delta l = \left(-D_0 \Delta c \cdot t\right)/\left(\Delta x C_{(Mg_2Si)}\right) \quad (6)$$

$c_{Mg_{36}Si_{15}Ni_{50}}$ is the concentration of Mg in $Mg_{36}Si_{15}Ni_{50}$ (3×10^{22} at./cm^3), t is aging time. According to the Mg-poor

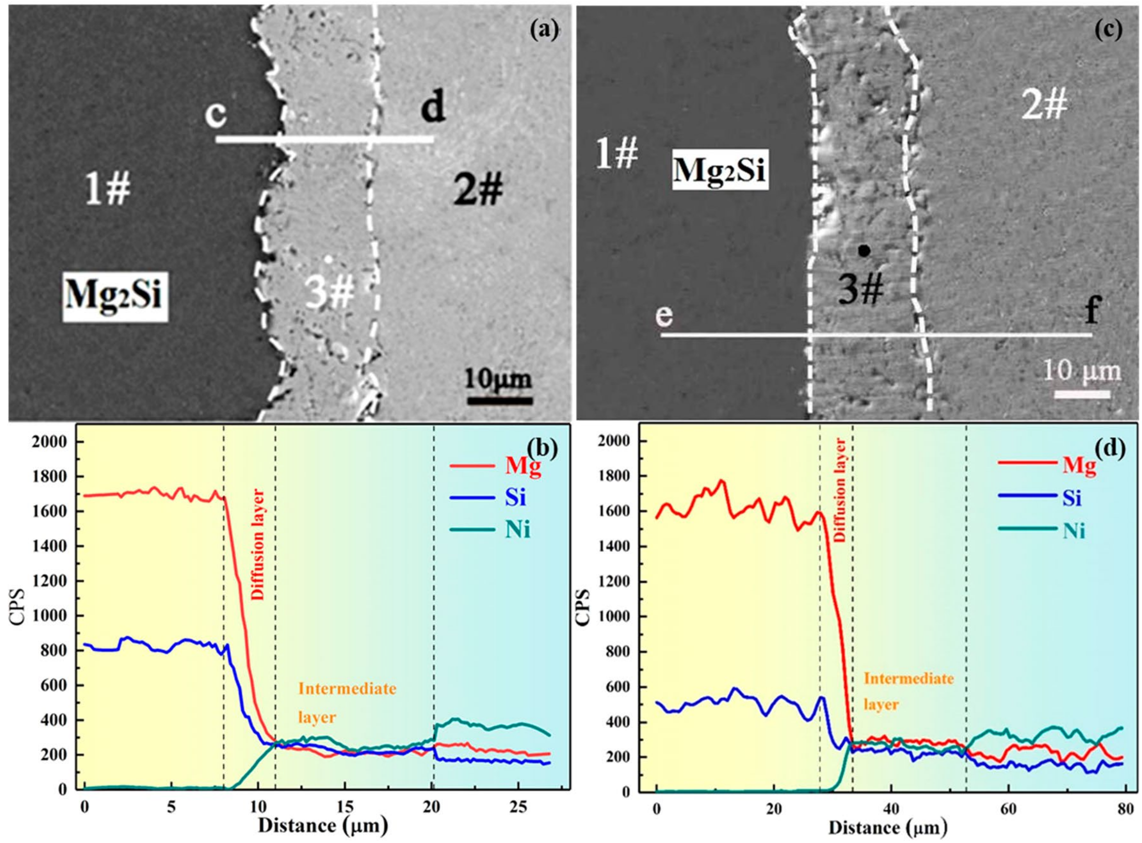

Fig. 5 Interface micromorphology and element distribution across the interface of (a), (b) $Mg_{130}Si_{15}Ni_{50}/Mg_2Si$ and (c) (d) $Mg_{50}Si_{15}Ni_{50}/Mg_2Si$.

layer thickness from Figs. 2 and 7, Δl is 4 μm. So, the diffusion coefficient of Mg from Mg_2Si to $Mg_{36}Si_{15}Ni_{50}$ at 400 ℃ is 2.15×10^{-12} cm^2/s. Compared with that[25] (2.0×10^{-10} cm^2/s) of Mg in the Mg_2Si at 500 °C , the diffusion coefficient of Mg from Mg_2Si to $Mg_{36}Si_{15}Ni_{50}$ at 400 ℃ was lower. For the interface of $Mg_2Si/Mg_{50}Si_{15}Ni_{50}$, $c_{Mg_{36}Si_{15}Ni_{50}}$ in $Mg_{50}Si_{15}Ni_{50}$(4.2×10^{22} at./cm^3). The direction of Mg concentration difference is from $Mg_{50}Si_{15}Ni_{50}$ to Mg_2Si. The results above indicate that increasing of Mg content of Mg_2SiNi_3 side can effectively suppress the Mg diffusion from Mg_2Si to Mg_2SiNi_3.

Interface Performance is Improved by Gradient Design

Contact resistivity has a significant effect on conversion efficiency and power output for thermoelectric modules,[33] which mainly depends on the interface microstructure as well as the electrical properties of the interfacial materials.[34–40] Lower contact resistivity ($R_C << L/2\sigma$) for thermoelectric joints is expected in long-term service.

Figure 6a shows the change of electrical resistance across the section of $Mg_xSi_{15}Ni_{50}/Mg_2Si$ (x=36,50,130) joints. The linearly increasing resistance on the Mg_2Si side indicates a semiconductor while that in the Mg_2SiNi_3 side indicates metallic property. An abrupt change between Mg_2SiNi_3 and intrinsic Mg_2Si can be observed, as summarized in Fig. 6a. The intrinsic contact resistance is 275.4 μΩ cm^2, 171.9 μΩ cm^2, 141.3 μΩ cm^2 for $Mg_{36}Si_{15}Ni_{50}/Mg_2Si$, $Mg_{50}Si_{15}Ni_{50}/Mg_2Si$, and $Mg_{130}Si_{15}Ni_{50}/Mg_2Si$, respectively, which are smaller than 320 μΩ cm^2 for the Mg_2Si/Ni joint measured by Sakamoto et al.[41] Compared with the $Mg_{36}Si_{15}Ni_{50}/Mg_2Si$ joint, the contact resistance of $Mg_xSi_{15}Ni_{50}/Mg_2Si$ joints (x=50, 130) is reduced by 50%. The higher contact resistivity of the $Mg_{36}Si_{15}Ni_{50}/Mg_2Si$ joint may be ascribed to the formation of MDR due to Mg diffusion.

To evaluate the interfacial reliability of the thermoelectric joints at high temperatures, aging tests of $Mg_xSi_{15}Ni_{50}/Mg_2Si$ (x=36, 50, 130) joints at 400 °C for 480 h are carried out. Figure 6b shows the change of contact resistance of $Mg_xSi_{15}Ni_{50}/Mg_2Si$ (x=36, 50, 130) joints after aging. These values are smaller than 16.4 mΩ cm^2 obtained for the Mg_2Si/Cu joint by Cai et al.[42] We conjecture that the increase in the contact resistivity with aging time might be ascribed to the loss vitalization of Mg of TE material during aging. Similar results have been reported in the literature.[20,24,43] The contact resistance of $Mg_{130}Si_{15}Ni_{50}/Mg_2Si$ and $Mg_{50}Si_{15}Ni_{50}/Mg_2Si$ are smaller than that of $Mg_{36}Si_{15}Ni_{50}/Mg_2Si$, indicating that

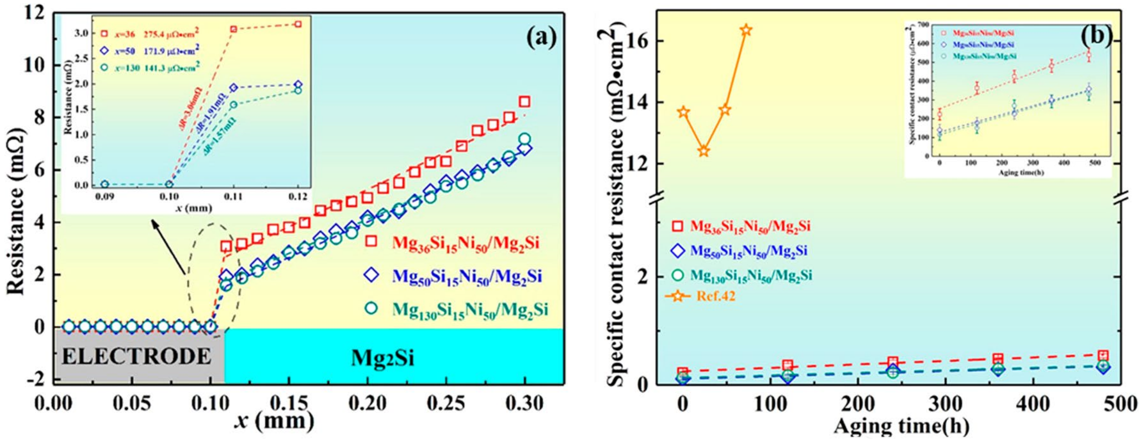

Fig. 6 (a) Testing curve of contact resistance of the joints (b) Variation of contact resistivity with different aging time for $Mg_xSi_{15}Ni_{50}/Mg_2Si$ (x = 36, 50, 130) joints.

the Mg-rich diffusion barrier layer can suppress the loss of Mg, thereby increasing the stability of the joint.

As shown in Fig. 7a, compared with that before aging in Fig. 2b, the phase component of the aged interface $Mg_{36}Si_{15}Ni_{50}/Mg_2Si$ after aging for 240 h is almost unchanged. But the thickness of the diffusion layer and MDR increases, where the thickness of the diffusion layer and MDR is around 20 µm and 11 µm, respectively (Fig. 7b). The increase in the MDR thickness may be ascribed to the diffusion layer which has inconspicuous inhibitory on the diffusion of Mg. Figure 7c and e shows the interface microstructure of $Mg_{50}Si_{15}Ni_{50}/Mg_2Si$ and $Mg_{130}Si_{15}Ni_{50}/Mg_2Si$ joints after aging at 400 °C for 240 h, respectively. Compared with that before aging, both the thickness and phase component remain unchanged.

The CTEs of Ni, $Mg_xSi_{15}Ni_{50}$(x=36, 50, 150) and Mg_2Si within the temperature range of 150-400 °C are shown in Fig. 8a. The CTE of Ni ranges from 13.2×10^{-6} K^{-1} to 14.8×10^{-6} K^{-1} between 150 °C and 400 °C,[20] that of $Mg_{36}Si_{15}Ni_{50}$ ranges from 12.1×10^{-6} K^{-1} to 11.2×10^{-6} K^{-1} , and that of $Mg_{50}Si_{15}Ni_{50}$ ranges from 11.3×10^{-6} K^{-1} to 13×10^{-6} K^{-1}, which is very close to that of $Mg_{130}Si_{15}Ni_{50}$.

Figure 8b shows that the resistivity decreases with increase of x. when x is greater than 50, it remains almost unchanged, and some liquid magnesium can be observed at the surface of the plunger (Fig. 3b), which indicates that no more magnesium may enter into the lattice. The Mg-Si-Ni ternary phase diagram[23] indicates that the residual Mg in $Mg_xSi_{15}Ni_{50}$(x=50, 130) exists as a second phase of Mg_2Ni at the grain boundary, with a CTE of 7.5×10^{-6} K^{-1} to 12.5×10^{-6} K^{-1} from 150 ℃ to 350 ℃,[20] which is far lower than that of $Mg_{36}Si_{15}Ni_{50}$.

Mg_2Si has a CTE within the scope of 10.2×10^{-6} K^{-1} and 18.9×10^{-6} K^{-1} from 150 °C to 400 °C.[20] The previous report showed that a CTE difference less than around 5-6 $\times10^{-6}$ K^{-1} does not lead to failure of the joint of Mg_2Si and Ni.[20] CTE of the barrier may be modified by changing the content of magnesium, which is beneficial to reduce the residual interface stress and improve the bonding strength and stability.

The shearing tests were conducted to evaluate the mechanical properties, as shown in Fig. 9. All of them are about 23 MPa before aging. These values are higher than that of 16.2 MPa and 19 MPa obtained for Mg_2Si/Cu and Mg_2Si/Ni joints by Cai et al[42] and Tohei et al.[44] Furthermore, this work shows great advantage after aging. As can be seen from Fig. 9, the strength of the $Mg_{36}Si_{15}Ni_{50}/Mg_2Si$ joint decreases more than the other two, which is mainly due to the phase component of the interface diffusion layer. The uniform and dense ω-phase diffusion layer at the interface of $Mg_xSi_{15}Ni_{50}/Mg_2Si$ (x=50, 130) can maintain high bonding strength during the aging. Additionally, the CTE difference (see Fig. 8) in interfaces is one of the reasons that the bonding strength decreases with aging time.[24]

Conclusions

In this work, Mg_2SiNi_3 (TCP-IMC) was selected as the barrier layer to bond with intrinsic Mg_2Si by SPS in one step. Adjusting the proportion of Mg in the barrier to suppress the migration of Mg across the interface thereby alleviates the degradation of the thermoelectric properties of the Mg_2Si thermoelectric material and increases the stability in service as well.

A diffusion layer was located between Mg_2Si and $Mg_{36}Si_{15}Ni_{50}$. The matrix is basically a mixture of Mg_2Si and Mg, with $NiSi_2$ precipitates as second phase. In the matrix of $Mg_xSi_{15}Ni_{50}/Mg_2Si$ (x=50, 130), a dense and uniform diffusion layer was observed, which was composed of an ω-phase (Mg:Si:Ni≈1:1:1) based on EDS and phase

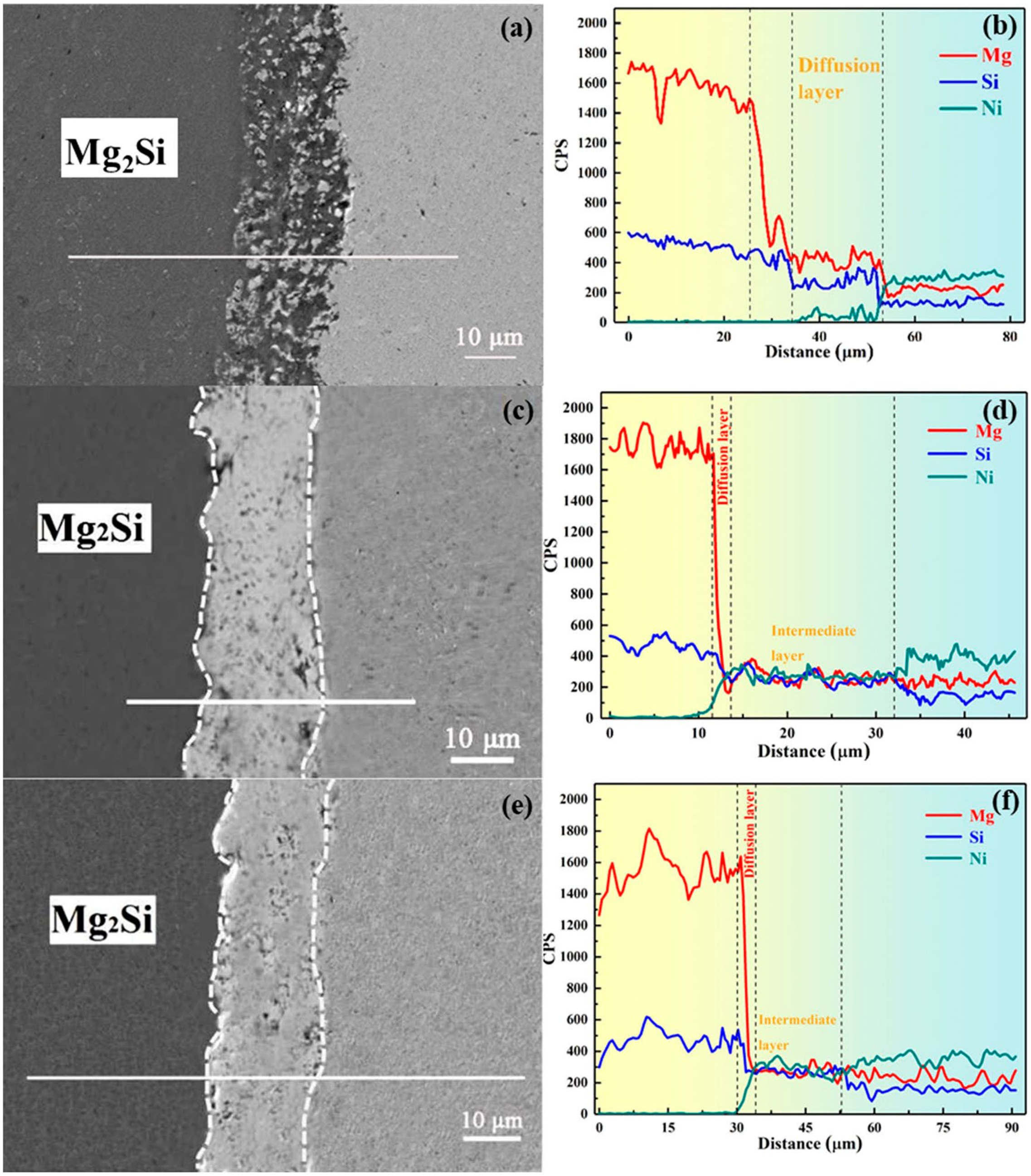

Fig. 7 Microstructure and EDS line scan analysis of $Mg_xSi_{15}Ni_{50}/Mg_2Si$ interface after annealing at 400 °C for 240 h (a), (b) $Mg_{36}Si_{15}Ni_{50}/Mg_2Si$ joint (c), (d) $Mg_{50}Si_{15}Ni_{50}/Mg_2Si$ joint (e) (f) $Mg_{130}Si_{15}Ni_{50}/Mg_2Si$ joint.

diagram. A higher chemical potential of Mg in the barrier is helpful to suppress the formation of the Mg-depletion layer in Mg_2Si.

The barrier of $Mg_xSi_{15}Ni_{50}$ (x=50, 130) effectively improves the interface conductivity and the bonding strength. The contact resistivity in $Mg_xSi_{15}Ni_{50}/Mg_2Si$ (x=50, 130) joints are 171.9 μΩ cm^2 and 141.3 μΩ cm^2, which are about 50% of that of $Mg_{36}Si_{15}Ni_{50}/Mg_2Si$ joint. The shear strength of all joints with different Mg content is around 23 MPa. $Mg_{50}Si_{15}Ni_{50}/Mg_2Si$ and $Mg_{130}Si_{15}Ni_{50}/Mg_2Si$ joints show better stability both in contact and shear strength after aging at 400 ℃ for different time.

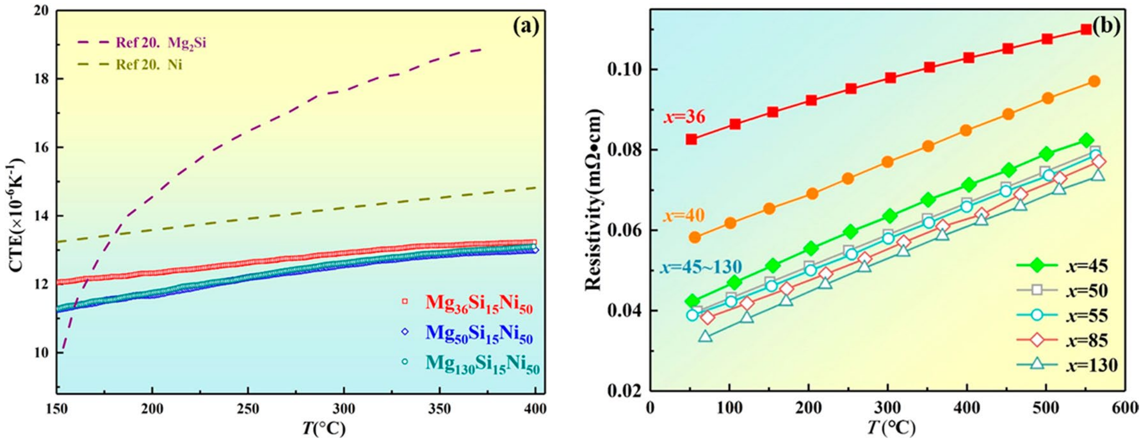

Fig. 8 (a) The CTE values of the $Mg_xSi_{15}Ni_{50}$(x = 36, 50, 150) (b) temperature dependence of resistivity of $Mg_xSi_{15}Ni_{50}$($36 \le x \le 130$) within the temperature range.

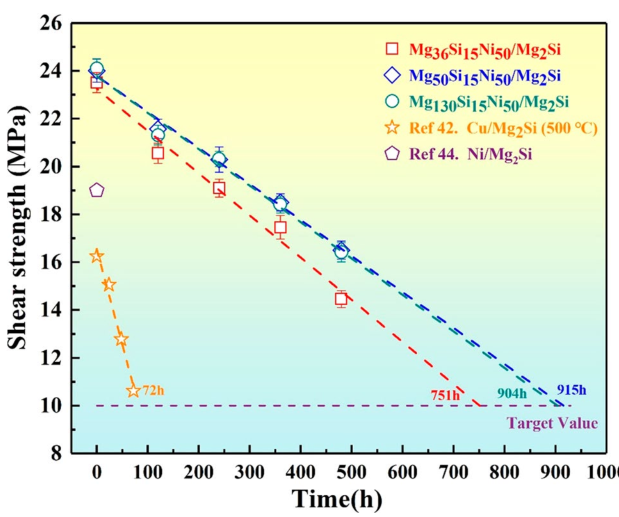

Fig. 9 The shear strength of $Mg_xSi_{15}Ni_{50}/Mg_2Si$ (x = 36, 50, 130) joints after aging.

Acknowledgments This work was supported by the National Science Foundation of China [No. 51775366, 51875387], the Shanxi Province Science Foundation through grant Nos. 201801D121017, 201901D111116, and the Shanxi Scholarship Council of China through grant Nos. 2017-050 and 2017-028.

Conflict of interest On behalf of all authors, the corresponding author states that there is no conflict of interest.

References

1. X.Y. Zhang, Z.L. Bu, S.Q. Lin, Z.W. Chen, W. Li, and Y.Z. Pei, GeTe Thermoelectrics. *Joule* 4, 986 (2020).
2. X. Shi, and J. He, Thermopower and harvesting heat. *Science* 371, 343 (2021).
3. J. de Boor, U. Saparamadu, J. Mao, K. Dahal, E. Muller, and Z.F. Ren, Thermoelectric performance of Li doped, p-type Mg2(Ge, Sn) and comparison with Mg2(Si, Sn). *Acta Mater.* 120, 273 (2016).
4. A. Kato, T. Yagi, and N. Fukusako, First-principles studies of intrinsic point defects in magnesium silicide. *J. Phys. Condens. Mat.* 21, 205801 (2009).
5. T.J. Zhu, Y.T. Liu, C.G. Fu, J.P. Heremans, J.G. Snyder, and X.B. Zhao, Compromise and synergy in high-efficiency thermoelectric materials. *Adv Mater.* 29, 1605884 (2017).
6. L. Yang, Z.G. Chen, M.S. Dargusch, and J. Zou, High performance thermoelectric materials: progress and their applications. *Adv. Energy Mater.* 8, 1701797 (2018).
7. J.Z. Xin, Y.L. Tang, Y.T. Liu, X.B. Zhao, H.G. Pan, and T.J. Zhu, Valleytronics in thermoelectric materials. *NPJ Quantum Mater.* 3, 1–9 (2018).
8. D. Champier, Thermoelectric generators: a review of applications. *Energ Convers. Manag.* 140, 167 (2017).
9. J.J. Kuo, Y. Yu, S.D. Kang, O. Cojocaru-Miredin, M. Wuttig, and G.J. Snyder, Mg deficiency in grain boundaries of n-Type Mg_3Sb_2 identified by atom probe tomography. *Adv. Mater. Interfaces* 6, 1900429 (2019).
10. W.S. Liu, H.Z. Wang, L.J. Wang, X.W. Wang, G. Joshi, G. Chen, and Z.F. Ren, Understanding of the contact of nanostructured thermoelectric n-type $Bi_2Te_{2.7}Se_{0.3}$ legs for power generation applications. *J. Mater. Chem. A* 1, 13093 (2013).
11. V.M. Sokolova, L.D. Dudkin, and L.I. Petrova, Diffusion processes at GeTe/SnTe/Fe contacts. *Inorga Mater.* 36, 16 (2000).
12. D.K. Aswal, R. Basu, and A. Singh, Key issues in development of thermoelectric power generators: High figure-of-merit materials and their highly conducting interfaces with metallic interconnects. *Energ. Convers. Manag.* 114, 50 (2016).
13. Y. Lu, Y. Qiu, Q.L. Jiang, K.F. Cai, Y. Du, H.J. Song, M.Y. Gao, C.J. Huang, J.Q. He, and D.H. Hu, Preparation and characterization of Te/Poly(3,4-ethylenedioxythiophene): poly(styrenesulfonate)/Cu_7Te_4 ternary composite films for flexible thermoelectric power generator. *ACS Appl. Mater. Interfaces* 10, 42310 (2018).
14. W.S. Liu, and S.Q. Bai, Thermoelectric interface materials: a perspective to the challenge of thermoelectric power generation module. *J. Materiomics* 5, 321 (2019).

15. X.M. Yang, S.P. Chen, H. Zhang, F. Lv, W.H. Fan, W.X. Wang, and Z.A. Munir, Thermoelectric properties and transport mechanism of pure and Bi-doped SiNWs-Mg_2Si. *Phys. Status Solidi A* 215, 1700742 (2018).
16. R. Santos, S.A. Yamini, and S.X. Dou, Recent progress in magnesium-based thermoelectric materials. *J. Mater. Chem. A* 6, 3328 (2018).
17. K. Yin, X.L. Su, Y.G. Yan, Y.H. You, Q. Zhang, C. Uher, M.G. Kanatzidis, and X.F. Tang, Optimization of the electronic band structure and the lattice thermal conductivity of solid solutions according to simple calculations: a canonical example of the $Mg_2Si_{1-x-y}Ge_xSn_y$ ternary solid solution. *Chem. Mater.* 28, 5538 (2016).
18. M. Wood, J.J. Kuo, K. Imasato, and G.J. Snyder, Improvement of low-temperature *zT* in a Mg_3Sb_2-Mg_3Bi_2 solid solution via Mg-vapor annealing. *Adv. Mater.* 31, e1902337 (2019).
19. T. Zhu, L. Hu, X. Zhao, and J. He, New insights into intrinsic point defects in V_2VI_3 thermoelectric materials. *Adv. Sci. (Weinh)* 3, 1600004 (2016).
20. S.P. Chen, Y.Z. Chen, S. Ohno, L.B. Xu, W.H. Fan, L. Xue, M. Ferhat, and Y.C. Wu, Enhancing interfacial properties of Mg_2Si-based thermoelectric joint with Mg_2SiNi_3 compound as electrodes. *Phys. Status Solidi A* 217, 1901035 (2020).
21. D. Noréus, L. Eriksson, L. Göthe, and P.E. Werner, Structure determination of Mg_2SiNi_3. *J. Less Common Metals* 107, 345 (1985).
22. L.B. Wang, D.J. Zhao, J.J. Lu, W.Q. Liu, and Q.F. Zhou, Solid-state synthesis and magnetic properties of rhombohedral phase Mg_2SiNi_3. *Int. J. Mater. Res.* 109, 177 (2018).
23. Y. Imai, H. Sugawara, Y. Mori, S. Nakamura, A. Yamamoto, and K.-I. Takarabe, Energetic consideration of compounds at Mg_2Si-Ni electrode interlayer produced by spark-plasma sintering. *Jpn. J. Appl. Phys.* 56, 05dc03 (2017).
24. R.Y. Yang, S.P. Chen, W.H. Fan, X.F. Gao, Y. Long, W.X. Wang, and Z.A. Munir, Interfacial properties of Cu/Ni/Mg_2Si joints prepared in one step by the spark plasma sintering method. *J. Alloys Compd.* 704, 545 (2017).
25. A. Kodentsov, A. Wierzbicka-Miernik, L. Litynska-Dobrzynska, P. Czaja, and J. Wojewoda-Budka, Formation of magnesium silicide in bulk diffusion couples. *Intermetallics* 114, 1–10 (2019).
26. D. Kato, K. Iwasaki, M. Yoshino, T. Yamada, and T. Nagasaki, Significant effect of Mg-pressure-controlled annealing: non-stoichiometry and thermoelectric properties of $Mg_{2-\delta}Si_{1-x}Sb_x$. *Phys. Chem. Chem. Phys.* 20, 25939 (2018).
27. M. Kubouchi, K. Hayashi, and Y. Miyazaki, Quantitative analysis of interstitial Mg in Mg_2Si studied by single crystal X-ray diffraction. *J. Alloys Compd.* 617, 389 (2014).
28. T. Dasgupta, C. Stiewe, R. Hassdorf, A.J. Zhou, L. Boettcher, and E. Mueller, Effect of vacancies on the thermoelectric properties of $Mg_2Si_{1-x}Sb_x$ ($0 \leq x \leq 01$). *Phys. Rev. B* 83, 235207 (2011).
29. P. Jund, R. Viennois, C. Colinet, G. Hug, M. Fevre, and J.C. Tedenac, Lattice stability and formation energies of intrinsic defects in Mg_2Si and Mg_2Ge via first principles simulations. *J. Phys. Condens. Mat.* 25, 035403 (2013).
30. X. Liu, L. Xi, W. Qiu, J. Yang, T. Zhu, X. Zhao, and W. Zhang, Significant roles of intrinsic point defects in Mg_2X(X= Si, Ge, Sn) thermoelectric materials. *Adv. Electron Mater.* 2, 1500284 (2016).
31. J. De Boor, D. Droste, C. Schneider, J. Janek, and E. Mueller, Thermal stability of magnesium silicide/nickel contacts. *J. Electron. Mater.* 45, 5313 (2016).
32. X.K. Hu, S.M. Zhang, F. Zhao, Y. Liu, and W.S. Liu, Thermoelectric device: contact interface and interface materials. *J. Inorg. Mater.* 34, 269 (2019).
33. K. Xiong, W.C. Wang, H.N. Alshareef, R.P. Gupta, J.B. White, B.E. Gnade, and K.J. Cho, Electronic structures and stability of Ni/Bi_2Te_3 and Co/Bi_2Te_3 interfaces. *J. Phys. D Appl. Phys.* 43, 115303 (2010).
34. X.Y. Yang, J.H. Wu, M. Gu, X.G. Xia, and L.D. Chen, Fabrication and contact resistivity of W-Si_3N_4/TiB_2-Si_3N_4/p-SiGe thermoelectric joints. *Ceram Int.* 42, 8044 (2016).
35. C.H. Wang, H.C. Hsieh, Z.W. Sun, V.K. Ranganayakulu, T.W. Lan, Y.Y. Chen, Y.Y. Chang, and A.T. Wu, Interfacial stability in Bi_2Te_3 thermoelectric joints. *ACS Appl. Mater. Inter.* 12, 27001 (2020).
36. D.G. Zhao, H.R. Geng, and L.D. Chen, Microstructure contact studies for skutterudite thermoelectric. *Int. J. Appl. Ceram Tech.* 9, 733 (2012).
37. G. Joshi, and B. Poudel, Efficient and robust thermoelectric power generation device using hot-pressed metal contacts on nanostructured half-heusler alloys. *J. Electron. Mater.* 45, 6047 (2016).
38. D.G. Zhao, H.R. Geng, and X.Y. Teng, Fabrication and reliability evaluation of $CoSb_3$/W-Cu thermoelectric element. *J. Alloys Compd.* 517, 198 (2012).
39. S.P. Feng, Y.H. Chang, J. Yang, B. Poudel, B. Yu, Z.F. Ren, and G. Chen, Reliable contact fabrication on nanostructured Bi_2Te_3-based thermoelectric materials. *Phys. Chem. Chem. Phys.* 15, 6757 (2013).
40. T.C. Holgate, L. Han, N.Y. Wu, E.D. Bojesen, M. Christensen, B.B. Iversen, N.V. Nong, and N. Pryds, Characterization of the interface between an Fe-Cr alloy and the p-type thermoelectric oxide $Ca_3Co_4O_9$. *J. Alloys Compd.* 582, 827 (2014).
41. T. Sakamoto, T. Iida, Y. Honda, M. Tada, T. Sekiguchi, K. Nishio, Y. Kogo, and Y. Takanashi, The use of transition-metal silicides to reduce the contact resistance between the electrode and sintered n-Type Mg_2Si. *J. Electron. Mater.* 41, 1805 (2012).
42. L.L. Cai, P. Li, P. Wang, Q. Luo, P.C. Zhai, and Q.J. Zhang, Duration of thermal stability and mechanical properties of Mg_2Si/Cu thermoelectric joints. *J. Electron. Mater.* 47, 2591 (2018).
43. L. Yin, C. Chen, F. Zhang, X.F. Li, F.X. Bai, Z.W. Zhang, X.Y. Wang, J. Mao, F. Cao, X.J. Chen, J.H. Sui, X.J. Liu, and Q. Zhang, Reliable N-type $Mg_{3.2}Sb_{1.5}Bi_{0.49}Te_{0.01}$/304 stainless steel junction for thermoelectric applications. *Acta Mater.* 198, 25 (2020).
44. T. Tohei, S. Fujiwara, T. Jinushi, and Z. Ishijima, Bondability of Mg_2Si element to Ni electrode using Al for thermoelectric modules. *IOP Conf. Ser. Mater. Sci. Eng.* 61, 012035 (2014).

Publisher's Note Springer Nature remains neutral with regard to jurisdictional claims in published maps and institutional affiliations.